NUCL SCI TECH (2016) 27:109
DOI 10.1007/s41365-016-0123-5

A facile and precise method for quantifying small–large/light-weighted molecular interaction system

Wan-Rong Li[1] · Pei Gong[1] · Yu-Xing Ma[1] · Hai-Yang Gao[1] · Xiao-Ling Yun[1] · Ming Yuan[1] · Yu-Shuang Liu[1] · Feng Zhang[1]

Received: 24 June 2016 / Revised: 4 August 2016 / Accepted: 12 August 2016 / Published online: 25 August 2016

Abstract It is significant to quantify the intermolecular physisorption extent in biomedical field. By taking the advantage of a significant difference from either sizes or weights, we introduced a combination of Scatchard equation and either ultracentrifugation or size exclusion chromatography to obtain both the binding constant and the number of binding sites by using bovine serum albumin and eosin B as models. Compared to the photoluminescence quenching-based methods like Stern–Volmer and Hill equations, the introduced method is not only more precise but also simpler and more straightforward for the operation. Moreover, the protein conformational changes and the corresponding theoretical binding mode with an atomic resolution were also studied by using three-dimensional fluorescence spectroscopy and molecular docking method, respectively. These comparative results could help scientists select right methods to study any interactions between two molecules with significant differences from either sizes or weights.

Keywords Bovine serum albumin · Eosin B · Binding constant · Ultracentrifugation · Scatchard equation · Size exclusion chromatography

1 Introduction

The intermolecular interactions play paramount roles in biological activities, and to learn the mechanisms created by mother nature needs to understand all the details of the interactions, especially for the binding constant and the number of binding sites, which could reversibly influence labeling, detecting/sensing, and therapy efficiencies. A number of methods have been developed to study intermolecular interactions, such as gel electrophoresis (GE) [1–4], electrochemistry [5], spectroscopy [1, 3, 4, 6–11], quartz crystal microbalance (QCM) [12–14], surface plasmon resonance (SPR) [15, 16], and also computer simulations [17, 18] are popularly used in biomedical field. In general, the raw data obtained by the above methods normally need to be further processed in combination with some classical equations like Stern–Volmer equation, Scatchard equation, and Hill equation to get the binding constants, sites and even cooperativities in order to comprehensively understand intermolecular interactions. Let's take a simple molecular interaction system as an example: $R + L \rightleftharpoons RL$, the binding constant can be described as $K_a = [RL]/([R][L])$, from which three concentrations must be figured out to calculate the final K_a. However, one may only know the concentrations of both [R] and [L] at the beginning of reaction. Alternatively, they could be indirectly obtained by subtracting the final concentration of [RL] from the initial concentration of [L] or [R] at the equilibrium state. Most of the above methods adapt to measuring the concentration of

This work was supported by the National Natural Science Foundation of China (Nos. 21171086 and 81160213), the Inner Mongolia Autonomous Region science and Technology Department (No. 211-202077), the Inner Mongolia Grassland Talent (No. 108-108038), the Natural Science Foundation of Inner Mongolia Autonomous Region of China (Nos. 2013MS1121, 2015ms0806 and 2016MS0211) and the Inner Mongolia Agricultural University (Nos. 109-108040, 211-109003 and 211-206038).

✉ Feng Zhang
fengzhang1978@hotmail.com

[1] Agricultural Nanocenter, School of Life Sciences, Inner Mongolia Agricultural University, 306 Zhaowuda Road, Hohhot 010018, China

[RL], such as spectroscopy-, QCM-, and SPR-based methods. However, the precision of results could be interfered somehow by the subtle deviations from the calibration curves made before binding. Hence, it will be more precise and reliable to directly measure the concentration of free [L] or [R] at the equilibrium.

Inspired by the separation principle of centrifugation and size exclusion chromatography (SEC) [19], we can learn that both these two separation methods are based on the significant intermolecular difference between either weights or sizes. It might not be a coincidence, and most of the important interactions in biomedical researches can make best use of this principle, especially for pharmaceutic researches since almost all of designed drugs are much smaller than what they really interact with in cells. With the deliberate calculation equation invented by an American chemist George Scatchard, we would like to demonstrate that the combination of Scatchard plot and ultracentrifugation/SEC can be a facile and more precise method to solve the binding constant and the number of binding sites for small–large/-light-weighted molecular interactions.

Eosin B (4′,5′-dibromo-2′,7′-dinitrofuorescein, EB) is a form of eosin dyes which belong to xanthenes class and have been used as histological stains [20], for protein estimations [21, 22], and sonosensitizers [23] for decades, and its analog eosin Y (EY) has been used for staining proteins on acid–urea polyacrylamide gels [24]. Bovine serum albumin (BSA), also known as "fraction V" which refers to the fifth separation fraction by using the original Edwin Cohn purification methodology, has been considered a model protein because it shares a high sequence homology of 76.52 % with human serum albumin (HSA) [3]. Serum albumin is the most abundant drug carrier protein in blood plasma playing an important role in the transportation and distribution for endogenous and exogenous substances.

In this work, BSA–EB interaction system has been studied by a comprehensive comparison of different methods since EB and BSA can be considered as the model small/large and large/weighted molecules, respectively. Firstly, a combination of Scatchard equation and either ultracentrifugation or SEC for the physisorption of BSA–EB was investigated. Secondly, other methods like combination of photoluminescence (PL) quenching and either Stern–Volmer equation or Hill equation have been introduced to make comparisons. In addition, the conformational changes of BSA upon binding EB have been studied by using three-dimensional fluorescence spectroscopy (3DFS), meanwhile, the binding mode of BSA–EB with atomic resolution was simulated by using molecular docking methods. We hope this study could contribute to the investigation of small/large molecular interaction system.

2 Experimental

2.1 Materials

BSA (Fraction V, lyophilized powder >98 %, Mw 66.5 kDa), EB (~90 %, Mw 590.09) and all other chemical regents were purchased from Sigma-Aldrich Corporation. Deionized water (18.2 MΩ cm) used for all experiments was made from a Milli-Q system (Millipore, Bedford, MA). Both BSA and EB molecules were dissolved in Milli-Q water for a stock solution with a concentration of 600 μM.

2.2 Spectroscopic measurements

Absorption spectra were recorded on a U-2900 UV–Vis spectrometer (Hitachi). PL spectra were recorded with a PL spectrometer (Fluorolog®-MAX 4, Horiba) equipped with a 1.0-cm quartz cell with a fixed excitation wavelength of 280 nm, and both excitation and emission slits were set up to 5 nm.

2.3 Ultracentrifugation, SEC, and PL quenching assays

The ultracentrifugation-based assays were conducted at 140, 000 rpm for 2 h with an ultracentrifuge (Hitachi, CS150FNX, Japan). The SEC assays were performed on a Sephacryl S-300 column equipped with a high-performance liquid chromatography (HPLC) system (Agilent 1260) with a flow phase of SB9 (sodium borate 50 mM, pH = 9) buffer and the flow rate of 1 mL/min, and the spectra monitored at both 280 nm for BSA and 516 nm for EB by a UV–Vis detector. The molar ratios of EB/BSA for both ultracentrifugation and SEC experiments are listed in Table 1, and the BSA's concentration was fixed to 3 μM. As to the fluorometric titration experiment, 800 μL solutions with different EB/BSA molar ratios were used for the measurement and the final BSA's concentration was fixed to 0.67 μM.

2.4 Calculation with different equations

Scatchard Eq. (1):

$$\frac{v}{C_{f(EB)}} = nK_a - vK_a \quad (1)$$

Table 1 EB/BSA molar ratios used for both ultracentrifugation and SEC experiments, and all mixtures were prepared and incubated at 298 K for 2 h

Vial number	BSA	EB
1	1	2
2	1	4
3	1	6
4	1	8
5	1	10

In Eq. (1), $C_{f(EB)}$ is the concentration of free ligand which is the unbound EB's concentration, and n is the number of binding sites per protein molecule. K_a is the association/binding constant/affinity of EB for BSA. The real bound ratio v can be obtained by Eq. (2).

$$v = \left(C_{t(EB)} - C_{f(EB)}\right)/C_{t(BSA)} \quad (2)$$

$C_{t(EB)}$ is the concentration of total EB which is known before the binding assay. $C_{f(EB)}$ is the free or unbound EB's concentration which can be obtained by either ultracentrifugation or SEC measurement. $C_{t(BSA)}$ is the concentration of total BSA for the binding assay, which is known and constant in the current assay.

2.5 Molecular docking

The three-dimensional (3D) structure of the BSA (PDB ID: 4JK4) was downloaded from Protein Data Bank (http://www.rcsb.org/pdb/home/home.do). The Auto Dock Tools 1.5.6 package (http://mgltools.scripps.edu) was employed to generate the docking input files. The important docking parameters were recorded as followings: The center x, y, and z coordinates of the search grid of BSA were 97.127, 24.933, and 20.919, respectively. And all of the x, y, and z dimension sizes were set as 15. The default parameters were used if it was not mentioned, and the best-scoring pose judged by the Vina docking score is chosen and visually analyzed using PyMOL software (http://www.pymol.org/).

3 Results and discussion

The absorption spectra comparison of BSA at 280 nm before and after ultracentrifugation has proved that the current ultracentrifugation condition is enough for a perfect separation of bound EB and free EB (Fig. 1a), and this has largely simplified both measurements and calculations: On one hand, normally an ultracentrifuge can contain at least six vials and this will be enough for the plot; on the other hand, one can just stop the centrifuge and take about no more than half supernatant from the vials for the concentration measurement simply with a lab pipette. With an absorption maximum dependent concentration calibration curve (Fig. 1b), the free EB's concentration can be calculated from the maximum absorption of supernatants (Fig. 1c) and thus the corresponding Scatchard plot curve can be obtained (Fig. 1d). With the slope and intercept from the best linear fit of the Scatchard plot, the K_a and

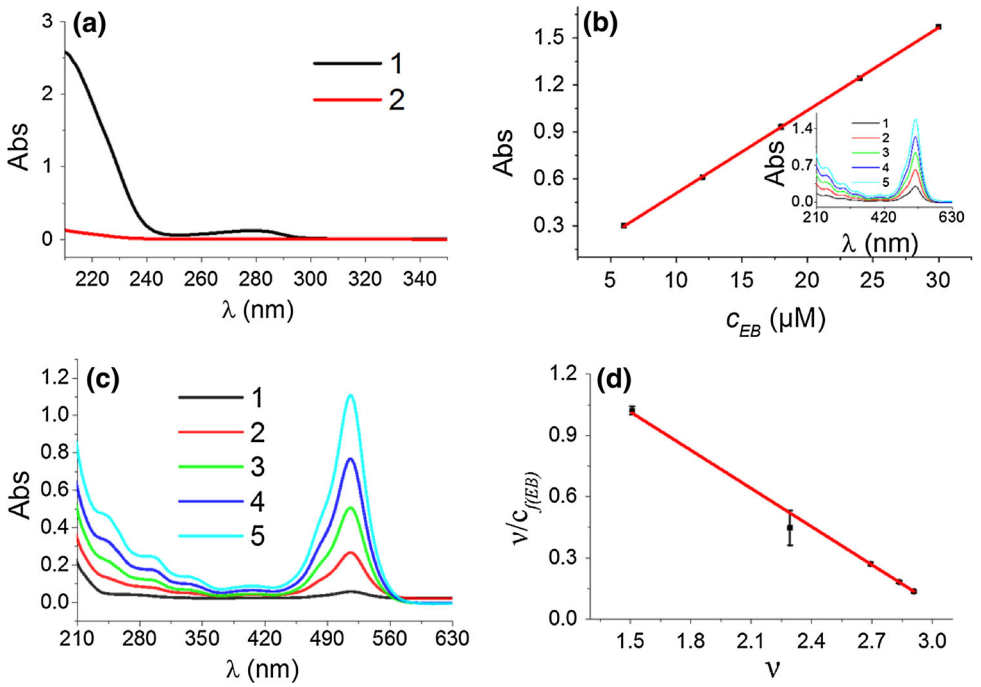

Fig. 1 Scatchard assay based on ultracentrifugation. **a** The absorption comparison between BSA before (*1*) and after (*2*) ultracentrifugation (140, 000 rpm for 2 h). **b** The plotted calibration curve of EB's absorption against concentration ($C_{f(EB)}$), and the inset is the absorption spectra of EB with varied concentrations as numbered from 5 to 1: 30, 24, 18, 12, 6 μM, respectively; all of the data points were averaged from three latest replicates with a standard error less than 0.2 %. **c** The absorption spectra of supernatants after the ultracentrifugation of BSA–EB mixture (the molar ratios from numbered 5–1 as: ½, ¼, 1/6, 1/8, and 1/10, respectively). **d** The plotted Scatchard curve (*black dots*) and the corresponding best linear fit (*red line*) of BSA–EB binding. The data were averaged from at least three replicates. (Color figure online)

number of binding sites were determined to 0.624 μM^{-1} (6.24×10^5 M^{-1}) and 3.11, respectively.

By using SEC, EB molecules can be also well repeatedly, precisely eluted during 20–40 min. One can see there are shoulder peaks at 24 min (Fig. 2a) of the elution spectra, which could be assigned to some micelle-like nanostructures formed by EB molecules due to the π–π interaction since it can be removed in the diluted solutions (lower than its critical micelle concentration). A calibration curve was then made by plotting the integrated eluted peaks against the elution time (Fig. 2b), which can facilitate the calculation of the free EB's concentration. With a control sample of free BSA, it can be clearly seen that BSA and BSA–EB cannot be separated with the current SEC columns (Fig. 2c). Similar to the ultracentrifugation method, the free EB's concentrations can be directly calculated from the SEC results by running the mixtures with the varied molar ratios of EB/BSA (as shown in Table 1) on HPLC. With calculations, another Scatchard equation can be plotted (Fig. 2d) and from which the binding constant K_a and the number of binding sites n were obtained as 0.57 μM^{-1} (5.7×10^5 M^{-1}) and 2.93, respectively.

In contrast to the Scatchard method, all of Stern–Volmer equation (Eq. 3), modified Stern–Volmer equation (Eq. 4) and Hill equation (Eq. 5) have been employed to analyze the binding constant as well, moreover, Hill equation can figure out the cooperativity in the binding procedure.

$$\frac{F_o}{F} = 1 + K_{SV}[Q] = 1 + k_q\tau_0[Q], \tag{3}$$

$$\frac{F_o}{F_o - F} = \frac{1}{f_a K_a}\frac{1}{[Q]} + \frac{1}{f_a}, \tag{4}$$

$$\log\frac{F_o - F}{F - F_{sat}} = \log K_a + n\log[Q], \tag{5}$$

where F_o, F, and F_{sat} are the PL intensities in the absence, presence, and saturated state of quencher, respectively. The Stern–Volmer quenching constant is given by $K_{SV} = k_q\tau_0$, where k_q is the quenching constant, τ_0 is the lifetime of the fluorophore in the absence of quencher, f_a, K_a, n, and $[Q]$ are the fraction of accessible fluorophores, the effective

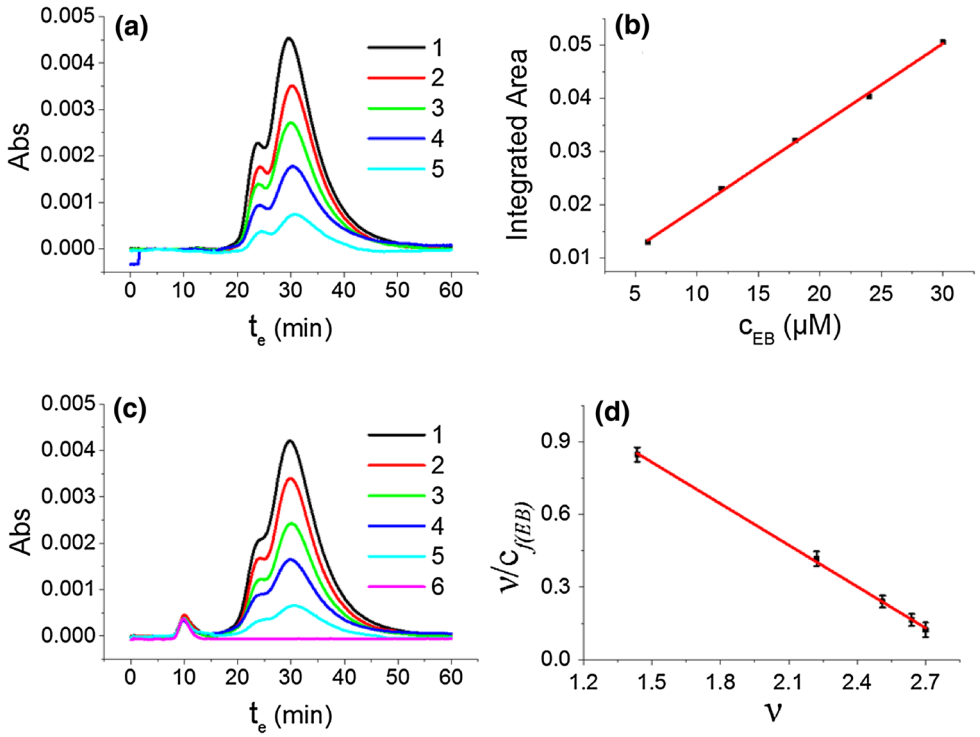

Fig. 2 Scatchard assay based on SEC. **a** The plotted curves of absorption at 516 nm against elution time (t_e) with the varied EB's concentrations as: 30, 24, 18, 12, 6 μM, respectively (from 1 to 5); **b** the plotted calibration curve and its best linear fit of EB's integrated absorption peaks against its concentration ($C_{f(EB)}$). The intercept and slope from the linear fit are 0.00408 and 0.00154, respectively. All of the data points were averaged from three replicates with a standard error less than 0.2 %. **c** The plotted SEC elution with the molar ratios of EB/BSA varied as 10/1, 8/1, 6/1, 4/1, 2/1, and 0/1, respectively (from 1 to 6); the peaks shown in the figure reflect the free EB's concentration ($C_{f(EB)}$), and the conjugate's concentration was too low compared to the free EB's to be seen in the figure, which is actually eluted out at 10 min; **d** The plotted Scatchard curve (*black dots*) and the corresponding best linear fit (*red line*) of EB binding to BSA based on (**c**). The intercept and slope from the linear fit are 1.67 and −0.57, respectively. The data were averaged from at least three replicates. (Color figure online)

quenching constant or the binding constant for the accessible fluorophores, the number of binding sites, and the concentration of the quencher, respectively (Table 2).

However, both Stern–Volmer and Hill equations-based methods require PL variations, for an example the PL quenching upon binding. Owning to spectra overlap between the BSA's PL and EB's absorption (Fig. 3a), the FRET can made best use to realize these two methods. To this end, the PL spectra were recorded for the mixtures with varied EB/BSA molar ratios (Fig. 3b), and the EB's PL range did not show up because of the strong interruption from the second harmonic peak (@560 nm which is very close to EB's PL @548 nm) of current excitation wavelength (280 nm), which has no real reference value since the measured samples were not purified. In practice, the Stern–Volmer plot showed a downwards bent curve (Fig. 3c inset), indicating a complicated binding procedure which most of time involves both static and dynamic quenching or even conformational changes upon binding [25]. Hence, a modified Stern–Volmer equation was plotted again with better linear results (Fig. 3c), and K_a and f_a were determined to $5.33 \times 10^6\ M^{-1}$, and 0.94, respectively. Similarly, by applying Hill equation to the corresponding data, a double logarithmic plot and its best linear fit (Fig. 3d) can give out $5.72 \times 10^4\ M^{-1}$ and 0.68 as an additional K_a and an important parameter for cooperativity n, respectively.

With comparison of several references' report, we think that both Scatchard-based ultracentrifugation and SEC results should approach the truth. However, in contrast to the Scatchard-based methods, the binding constant K_a deduced from FRET-based methods is not well stable, because the difference of K_a values deduced from modified Stern–Volmer and Hill equations was around two orders of magnitude, though that f_a is less one (Table 2) makes much sense (the accessible fraction of EB to BSA cannot be more than one). We attribute this huge deviation to the unstable PL of BSA due to the confirmation changes of BSA upon binding with EB. To further study the conformational information of BSA, we have employed 3DFS to see whether BSA conformation changes.

3DFS is a facile and powerful method to provide more detailed information about the conformational and

Table 2 Comparison of results derived from different methods

Principle	Ultracentrifugation		FRET/PL quenching	
Equation	Scatchard	SEC	Modified Stern–Volmer	Hill
K_a (M^{-1})	6.24×10^5	5.70×10^5	5.33×10^6	5.72×10^4
n	3.11	2.93	–	0.68
f_a	–	–	0.94	–

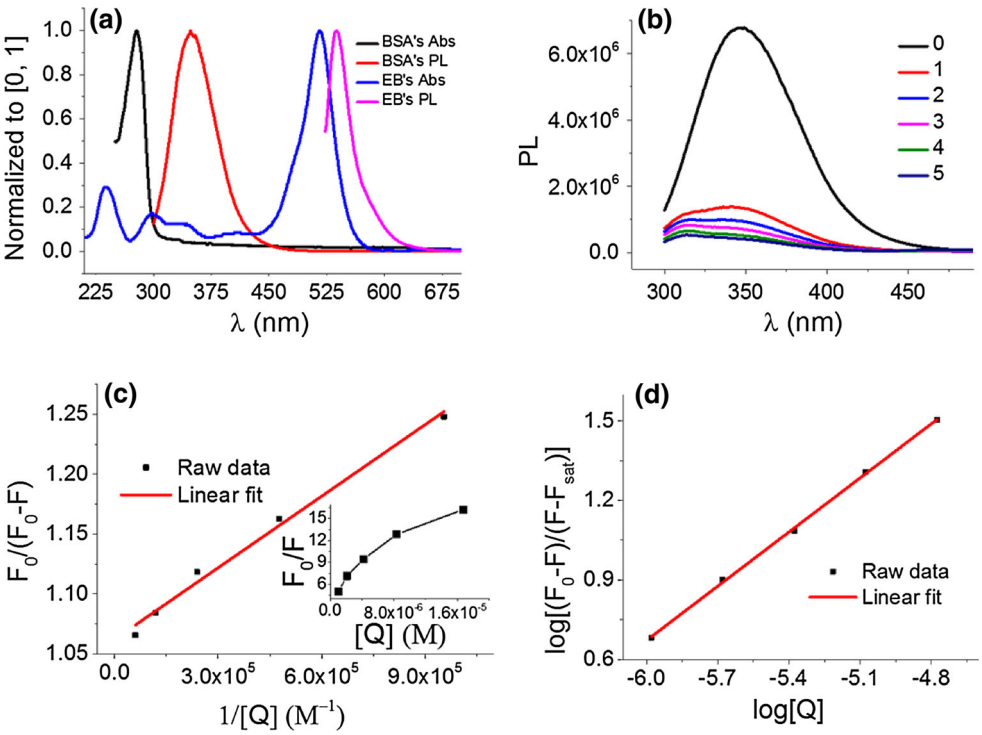

Fig. 3 Spectroscopy assay of BSA–EB interactions. a) Both absorption and emission spectra of free EB and BSA; **b** The PL quenching of BSA by EB with different mixing molar ratios of EB/BSA (from 5 to 0 are: 25, 12.5, 6.3, 3.2, 1.6, 0, respectively) showed a Förster resonance energy transfer (FRET) phenomenon; based on the PL quenching of BSA from (**b**), the Stern–Volmer plot (*inset* is the modified) in (**c**) and the Hill double logarithm plot (*black dots*) and its corresponding best linear fit in (**d**) were drawn

microenvironmental changes of protein that combined with molecules [1, 7, 10]. The principle of 3DFS is based on that the intrinsic fluorophores (like Trp residues) in proteins, whose PL can be strongly influenced by the polarity of the local environment. For example, the PL of a protein containing a single Trp in its hydrophobic core will be red-shifted upon exposure this Trp to an aqueous environment [26]. From Fig. 4, two typical PL peaks can be clearly observed in the 3DFS of BSA (peak 1: $\lambda_{ex}/\lambda_{em}$ = 276 nm/346 nm, peak 2: $\lambda_{ex}/\lambda_{em}$ = 244 nm/350 nm). Refers to the previous report [27], peak 1 mainly reveals the spectral characteristics of Trp and Tyr residues, is the primary PL peak, while peak 2 may mainly exhibit the PL characteristic of polypeptide backbone structures; therefore, its PL intensity can be correlated with the secondary structure of proteins. The corresponding spectral parameters were summarized in Table 3. Combining Fig. 4 with Table 3, it is clear to see that both PL intensities of peak 1 and peak 2 of BSA decrease with the gradual addition of EB, whereas the Rayleigh scattering peak is almost unchanged. Analyzing from the intensity changes of both peak 1 and peak 2, the quenching results indicated that the interaction of EB with BSA induced a slight unfolding of the protein polypeptides, resulting in a conformational change of the protein, and this could increase the exposure region of some hydrophobic regions that have previously been buried. Moreover, we realized that the maximum of PL of BSA occurred a blueshift due to water Ramon peak, which might be the one of the main reasons that cause the huge deviation of results obtained from two PL quenching-based methods.

With the aim to get the detailed binding site information at the atomic level, the molecular docking method [19] was employed by using Auto dock software package. As shown in Fig. 5, EB can be perfectly docked into the binding pocket of the BSA. The benzoic acid ring of EB fits into bottom of the binding pocket of BSA, surrounded by the residues Trp^{213}, Arg^{217}, Arg^{194}, and Arg^{198}. Detailed

Table 3 Summarized 3DFS parameters of EB binding to BSA

EB/BSA molar ratios	Peak 1			Peak 2		
	Peak position $\lambda_{ex}/\lambda_{em}$ (nm/nm)	Stokes shift $\Delta\lambda$ (nm)	I_F*	Peak position $\lambda_{ex}/\lambda_{em}$ (nm/nm)	Stokes shift $\Delta\lambda$ (nm)	I_F*
0	276/345	69	1.88×10^6	236/351	115	4.38×10^5
2	276/346	70	1.66×10^6	244/346	102	3.78×10^5
4	276/346	70	1.40×10^6	244/350	106	3.21×10^5
8	276/344	68	9.65×10^5	248/346	98	2.76×10^5

* I_F is the PL intensity from the 3DFS

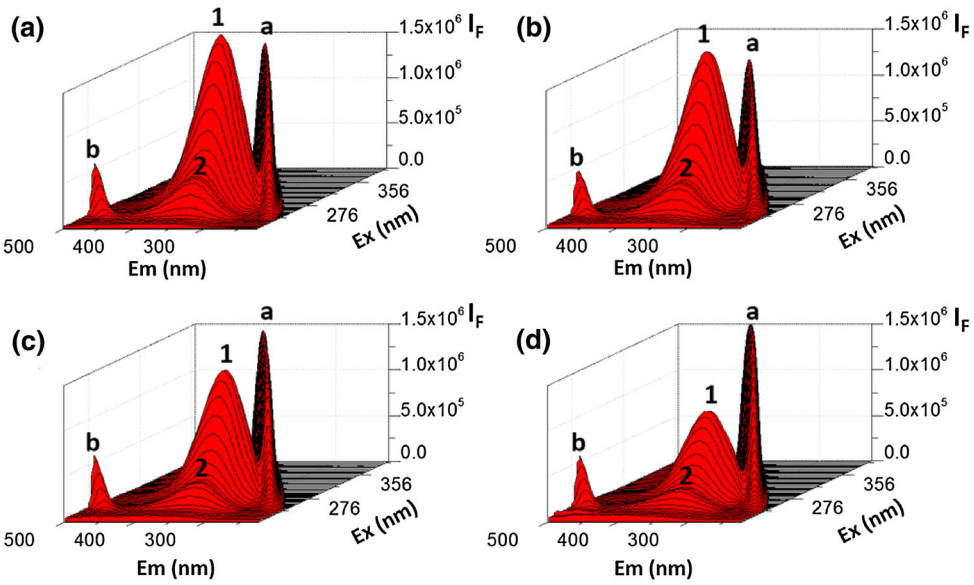

Fig. 4 Three-dimensional excitation and emission matrix of BSA upon binding to EB. **a** is for BSA alone; **b**–**d** are for the samples with different EB/BSA molar ratios as 2, 4, and 8, respectively. Peak a and b are two Rayleigh scattering peaks with its emission wavelength equals to and is two times (second-ordered harmonics) as its excitation wavelength, respectively. The *number 1* and *2* indicate two peaks with the wavelengths of excitation/emission are 276/346 and 244/350 nm, respectively

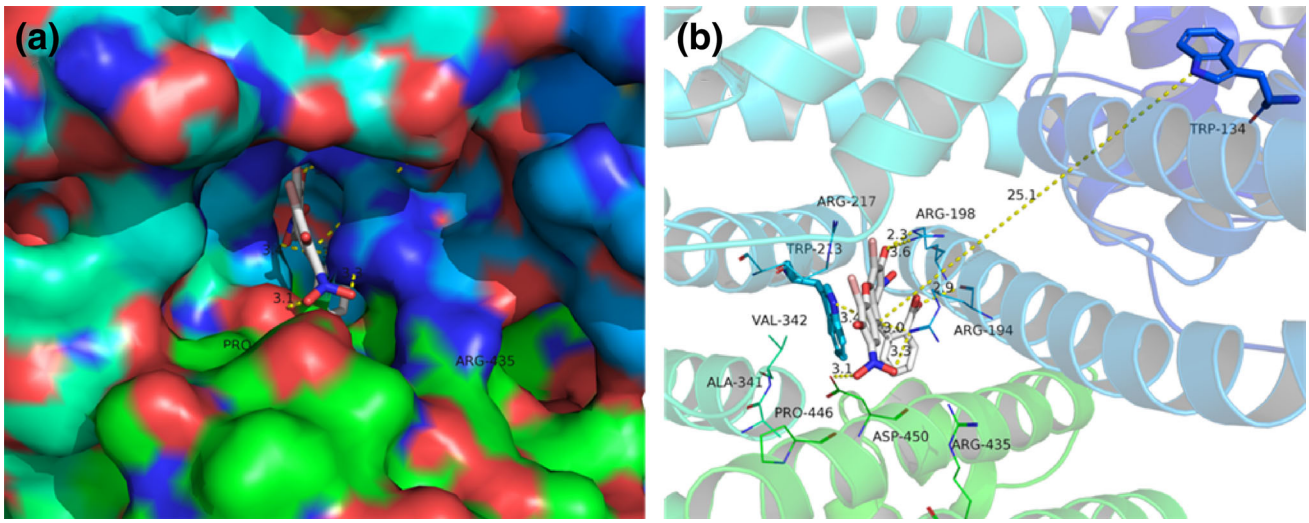

Fig. 5 Molecular docking of EB binding to BSA. **a** The EB is docked into the binding pocket of the BSA. **b** The detailed analysis of main binding sites between BSA's amino acid residues and EB structure. The unit of all distances is Å (0.1 nm)

analysis shows that carboxy group forms a hydrogen bond (2.9 Å) with residue Arg^{198}. Furthermore, carbonyl oxygen forms two hydrogen bonds (2.3 and 3.6 Å) with residue Arg^{198}, while the nitro group forms two hydrogen bonds (3.1 and 3.3 Å) with residue Asp^{450} and Arg^{194}, respectively, which could be the main binding affinity between EB and BSA.

4 Conclusion

A combinational method has been introduced to successfully quantifying the model BSA–EB interaction by taking the advantages of significant differences of either sizes or weights. In comparison with PL quenching-based methods, the current introduced methods are simpler to operate and can produce more precise results. In addition, the conformational changes of BSA upon binding EB and the atomic resolved theoretical binding mode were studied by 3DFS and molecular docking method, respectively. The introduced facile method could be widely applied for bio-drug interaction researches or any two substances with large difference in sizes or weights. This study has also provided a good demonstration to the well combination of experimental measurements and the theoretical simulations.

References

1. J. Guo, R.B. Zhong, W.R. Li et al., Interaction study on bovine serum albumin physically binding to silver nanoparticles: evolution from discrete conjugates to protein coronas. Appl. Surf. Sci. **359**, 82 (2015). doi:10.1016/j.apsusc.2015.09.247
2. R.B. Zhong, M. Yuan, H.Y. Gao et al., A subtle calculation method for nanoparticle's molar extinction coefficient: the gift from discrete protein-nanoparticle system on agarose gel electrophoresis. Funct. Mater. Lett. **9**, 1650029 (2016). doi:10.1142/S1793604716500296
3. Y.S. Liu, R.B. Zhong, P. Zhang et al., Understanding the robust physisorption between bovine serum albumin and amphiphilic polymer coated nanoparticles. ACS Appl. Mater. Interfaces **8**, 2478 (2016). doi:10.1021/acsami.5b08386
4. R.B. Zhong, Y.S. Liu, P. Zhang et al., Discrete nanoparticle-BSA conjugates manipulated by hydrophobic interaction. ACS Appl. Mater. Interfaces **6**, 19465 (2014). doi:10.1021/Am506497s
5. T.G. Drummond, M.G. Hill, J.K. Barton, Electrochemical DNA sensors. Nat. Biotechnol. **21**, 1192 (2003). doi:10.1038/nbt873
6. P. Wang, R.B. Zhong, M. Yuan et al., Mercury (II) detection by water-soluble photoluminescent ultra-small carbon dots synthesized from cherry tomatoes. Nucl. Sci. Tech. **27**, 35 (2016). doi:10.1007/s41365-016-0038-1
7. Z.J. Bai, Y.S. Liu, P. Zhang et al., Fluorescence resonance energy transfer between bovine serum albumin and fluoresceinamine. Luminescence **31**, 688 (2016). doi:10.1002/bio.3012
8. M. Yuan, R.B. Zhong, X.L. Yun et al., A fluorimetric study on the interaction between a Trp-containing beta-strand peptide and amphiphilic polymer-coated gold nanoparticles. Luminescence **31**, 47 (2016). doi:10.1002/bio.2920
9. R.B. Zhong, Y.S. Liu, P. Zhang et al., A facile method to build a proton nanosensor with neutral to basic pH sensitive range. Nucl. Sci. Tech. **25**, 040503 (2014). doi:10.13538/j.1001-8042/nst.25.040503
10. M. Yuan, R.B. Zhong, H.Y. Gao et al., One-step, green, and economic synthesis of water-soluble photoluminescent carbon dots by hydrothermal treatment of wheat straw, and their bio-applications in labeling, imaging, and sensing. Appl. Surf. Sci. **355**, 1136 (2015). doi:10.1016/j.apsusc.2015.07.095
11. Y.S. Liu, P. Zhang, R.B. Zhong et al., Fluorimetric study on the interaction between fluoresceinamine and bovine serum albumin. Nucl. Sci. Tech. **26**, 030505 (2015). doi:10.13538/j.1001-8042/nst.26.030505
12. K. Matsumoto, B.D.B. Tiu, A. Kawamura et al., QCM sensing of bisphenol A using molecularly imprinted hydrogel/conducting polymer matrix. Polym. J. **48**, 525 (2016). doi:10.1038/pj.2016.23

13. G.S. Huang, M.T. Wang, M.Y. Hong, A versatile QCM matrix system for online and high-throughput bio-sensing. Analyst **131**, 382 (2006). doi:10.1039/b515722f
14. R.B. Towery, N.C. Fawcett, P. Zhang et al., Genomic DNA hybridizes with the same rate constant on the QCM biosensor as in homogeneous solution. Biosens. Bioelectron. **16**, 1 (2001). doi:10.1016/S0956-5663(00)00126-3
15. H.A. Atwater, A. Polman, Plasmonics for improved photovoltaic devices. Nat. Mater. **9**, 205 (2010). doi:10.1038/nmat2629
16. J.N. Anker, W.P. Hall, O. Lyandres et al., Biosensing with plasmonic nanosensors. Nat. Mater. **7**, 442 (2008). doi:10.1038/nmat2162
17. F. Leo, A. Magistrato, D. Bonifazi, Interfacing proteins with graphitic nanomaterials: from spontaneous attraction to tailored assemblies. Chem. Soc. Rev. **44**, 6916 (2015). doi:10.1039/c5cs00190k
18. A.C. Newton, J. Groenewold, W.K. Kegel et al., Rotational diffusion affects the dynamical self-assembly pathways of patchy particles. Proc. Natl. Acad. Sci. USA **112**, 15308 (2015). doi:10.1073/pnas.1513210112
19. Y.X. Ma, R.B. Zhong, J. Guo et al., A facile method for studying interaction of rhodamine B and bovine serum albumin: towards physical-binding mediated fluorescence labeling of proteins. Nucl. Sci. Tech. **26**, 060502 (2015). doi:10.13538/j.1001-8042/nst.26.060502
20. D. Stefanovic, M. Stefanovic, D. Lalosevic, Use of eriochrome cyanine R in routine histology and histopathology: is it time to say goodbye to hematoxylin? Biotech. Histochem. **90**, 461 (2015). doi:10.3109/10520295.2015.1057765
21. A.A. Waheed, K.S. Rao, P.D. Gupta, Mechanism of dye binding in the protein assay using eosin dyes. Anal. Biochem. **287**, 73 (2000). doi:10.1006/abio.2000.4793
22. A.A. Waheed, P.D. Gupta, Single-step method for estimating nanogram quantities of protein. Anal. Biochem. **275**, 124 (1999). doi:10.1006/abio.1999.4301
23. L.L. He, X.X. Wu, Y.X. Wang et al., Spectroscopic investigation on the sonodynamic damage to protein in the presence of eosine B. Ultrason. Sonochem. **26**, 93 (2015). doi:10.1016/j.ultsonch.2015.02.002
24. A.A. Waheed, P.D. Gupta, Estimation of submicrogram quantities of protein using the dye eosin Y. J. Biochem. Biophys. Methods **42**, 125 (2000). doi:10.1016/S0165-022X(99)00055-X
25. J.R. Lakowicz, *Principles of Fluorescence Spectroscopy*, 3rd edn. (Springer, New York, 2006)
26. A. Grinvald, I.Z. Steinberg, The fluorescence decay of tryptophan residues in native and denatured proteins. Biochim. Biophys. Acta **427**, 663 (1976). doi:10.1016/0005-2795(76)90210-5
27. H.H. Sun, J. Zhang, Y.Z. Zhang et al., Interaction of human serum albumin with 10-hydroxycamptothecin: spectroscopic and molecular modeling studies. Mol. Biol. Rep. **39**, 5115 (2012). doi:10.1007/s11033-011-1307-z